Annals of Nuclear Medicine Vol. 18, No. 8, 659–667, 2004

Accuracy and reproducibility of co-registration techniques based on mutual information and normalized mutual information for MRI and SPECT brain images

Takashi YOKOI,*[1] Tsutomu SOMA,*[2,*3] Hiroyuki SHINOHARA*[4] and Hiroshi MATSUDA*[5]

*[1]*Image Processing Division, Bioimaging Laboratory, Inc.*
*[2]*Department of Medical Engineering, Division of Applied Health Sciences, Osaka University Medical School*
*[3]*Clinical Application Technology Group, Daiichi Radioisotope Laboratories*
*[4]*Department of Radiological Sciences, Tokyo Metropolitan University of Health Sciences*
*[5]*Department of Nuclear Medicine, Saitama Medical School Hospital*

We implemented a 3D co-registration technique based on mutual information (MI) including 2D image matching as a coarse pre-registration. The 2D coarse pre-registration was performed in the transverse, sagittal and coronal planes sequentially, and all six parameters were then optimized as fine registration. Normalized mutual information (NMI) was also examined as another entropy-based measure that was invariant to the overlapped area of two images. In order to compare accuracy and precision of the present method with a conventional two-level multiresolution approach, simulation was performed by 100 trials with the random initial mismatch of ±10° and ±17.92 mm (Type-I) and ±20° and ±40.32 mm (Type-II). For Type-I, no significant differences were found between registration errors of the multiresolution approach and the present method with the MI criterion. No biases were observed (≤0.13° and ≤0.57 mm for the multiresolution approach; ≤0.12° and ≤0.57 mm for the present method) and the SDs were very small (≤0.18° and ≤0.12 mm for the multiresolution approach; ≤0.11° and ≤0.11 mm for the present method). For Type-II, SDs for the multiresolution approach (≤1.8° and ≤0.88 mm) were markedly larger than those for the present method (≤0.64° and ≤0.20 mm) with MI. Success rate for the present method was 99.9%, which was higher than 97.6% for the multiresolution approach. Simulation also revealed that MI and NMI performance were almost equivalent. The choice of optimization strategy more affected accuracy and reproducibility than the choice of the registration criterion (MI or NMI) in our simulation condition. The present method is sufficiently accurate and reproducible for MRI-SPECT registration in clinical use.

Key words: image registration, mutual information, normalized mutual information, entropy, single photon emission computed tomography (SPECT)

INTRODUCTION

AUTOMATIC IMAGE REGISTRATION TECHNIQUE is becoming an increasingly important clinical tool in single-photon emission computed tomography (SPECT) and positron emission tomography (PET). Magnetic resonance imaging (MRI) and X-ray computed tomography (CT) provide anatomical information mostly without functional information. On the other hand, SPECT and PET provide functional information, but do not delineate anatomical information. After registration, these two modalities are fused into one image to obtain functional information localized over the anatomical images.[1–3] That registration technique has been applied toward attenuation correction in SPECT/PET using CT/MRI images that were geometrically aligned to the SPECT/PET images.[4–6]

Received May 25, 2004, revision accepted August 2, 2004.
For reprint contact: Takashi Yokoi, Ph.D., Bioimaging Laboratory, 22–6–107 Nishi-kyogoku Higashi-cho, Ukyo-ku, Kyoto 615–0816, JAPAN.
E-mail: tyokoi@bioimaging-lab.com

Table 1 List of image file parameters

Subject No.		Modality	Dimension	Voxel size (mm)
1	Normal	MRI-T1	256 × 256 × 59	1.23 × 1.23 × 2.10
		ECD-SPECT	128 × 128 × 92	2.46 × 2.46 × 2.46
2	Normal	MRI-T1	256 × 256 × 61	1.23 × 1.23 × 2.10
		ECD-SPECT	128 × 128 × 73	2.46 × 2.46 × 2.46
3	Ictal/Interictal	MRI-T1	256 × 256 × 57	1.23 × 1.23 × 2.24
		ECD-SPECT	128 × 128 × 51	2.46 × 2.46 × 2.46
		ECD-SPECT	128 × 128 × 54	2.46 × 2.46 × 2.46
4	Normal	MRI-T1	256 × 256 × 60	1.23 × 1.23 × 2.46
		ECD-SPECT	128 × 128 × 86	2.46 × 2.46 × 2.46
5	Normal	MRI-T1	256 × 256 × 52	1.23 × 1.23 × 2.46
		ECD-SPECT	128 × 128 × 80	2.46 × 2.46 × 2.46
6	Normal	MRI-T1	256 × 256 × 52	1.23 × 1.23 × 2.75
		ECD-SPECT	128 × 128 × 59	2.46 × 2.46 × 2.46
7	Normal	MRI-T1	256 × 256 × 41	1.23 × 1.23 × 2.75
		ECD-SPECT	128 × 128 × 51	2.46 × 2.46 × 2.46

Many approaches exist for 3-dimensional (3D) multimodal medical image registration. Most approaches are based on the mathematical framework of optimizing an intensity-based cost function. For example, Woods et al.[7] have proposed a method (AIR, automatic image registration) based on the minimization of the weighted sum of the standard deviation of intensities of PET voxels corresponding to narrow gray scale ranges of MRI-voxel intensities. Ardekani et al.[8] proposed a similar registration technique, called AMIR (automatic medical image registration), which uses the *K*-mean clustering algorithm to segment the MRI images into eight ranges of intensity and applied connected component analysis. Two images were then aligned by minimizing the variance of the PET/SPECT intensity within the segments. Performance comparisons of these approaches have been reported.[9–11] Recently, mutual information (MI) as the registration criterion was introduced independently by both Collignon et al.[12] and Viola and Wells,[13] and this idea was expanded by Maes et al.[14] AIR and AMIR are designed specifically for functional to anatomical image registration, whereas the MI is more general. The MI-based registration technique requires neither segmentation nor any ad-hoc assumptions about the properties of the imaging modalities. Validation of this algorithm has been reported for MRI-CT,[14,15] MRI-PET,[14,16] CT-transmission CT[17] and MRI-SPECT[18,19] studies. However, Studholme et al.[20] pointed out that MI is sensitive to the overlap area between the two images. They proposed normalized mutual information (NMI) as an alternative entropy-based measure that is invariant to the overlapped region of the two images. The NMI has also been used in a large number of studies.[21–23]

Many issues can affect MI- and NMI-based registration technique performance, including the optimization algorithm, number of bins of joint histogram, interpolation method, multiresolution and subsampling strategy. The multiresolution approach and the subsampling approach can improve the registration speed. In these techniques, registration is performed first at lower image resolution. Subsequently, the registration proceeds at higher image resolution. These approaches not only improve the computational efficiency, they also avoid trapping to local optima. In this study, we propose an alternative approach of 3D MI- and NMI-based registration technique that includes a 2D image matching as a coarse pre-registration with relatively few parameters. The present method was compared with the conventional coarse-to-fine multiresolution approach; its accuracy and reproducibility were evaluated with simulation data and clinical data sets of MRI and ^{99m}Tc-ethyl cysteinate dimmer (ECD) SPECT images.

METHODS AND MATERIALS

Mutual information and normalized mutual information

Mutual information $MI(A,B)$ is an index of how much information one random variable (A) tells about another (B); it is expressed as $MI(A,B) = H(A) + H(B) - H(A,B)$, where $H(A)$ and $H(B)$ are the Shannon's entropy[24] of A and B, and $H(A,B)$ is the joint entropy of A and B. $H(A)$, $H(B)$ and $H(A,B)$ can be computed from the 2D histogram of the intensity or gray values of two images.[14]

Normalized mutual information (NMI)[20] has also been proposed as another entropy-based measure that is invariant to the overlapped region of two images; it is defined as $NMI(A,B) = (H(A) + H(B))/H(A,B)$. This study examines the two similarity measures for the MRI-SPECT image registration. The procedure of image registration based on MI and NMI is described in the Appendix.

Implementation and optimization algorithm

The algorithm is assumed to be a rigid-body transformation involving six parameters that specify x-, y-, and z-axis rotations ($d\theta x$, $d\theta y$, $d\theta z$) and translations (dx, dy, dz). The

parameters are optimized such that the $MI(A,T(B))$ or $NMI(A,T(B))$ is maximized, where A and B is the reference (MRI) and the floating (SPECT) volume, respectively, and T is the transformation matrix. Trilinear interpolation and inverse mapping scheme is used to compute the voxel value in the floating volume to the corresponding voxel value in the reference volume. Gauss smoothing (FWHM = 8–10 mm) is applied to remove statistical noise on the SPECT images. Binning of the 2D histogram is performed on the two images as a preprocessing step. Linear binning employs a simple rescaling of the gray-scale range into the bin size of 64.

The Nelder-Mead Simplex algorithm[25,26] is used to search for the optimal parameters. This study examines two different optimization approaches. First, the two-level multiresolution approach[14,16,18] is examined as the standard registration technique to optimize the six parameters simultaneously. Resolution is changed from 1/2 to the original size. Secondly, we implement an alternative approach involving 2D image matching as a coarse pre-registration in the transverse plane ($d\theta z$, dx, dy), sagittal plane ($d\theta x$, dy, dz) and the coronal plane ($d\theta y$, dx, dz); all six parameters are then optimized as the fine registration. Coarse 2D pre-registration is performed using a halved resolution. Figure 1 illustrates the 2D pre-registration strategy in the present method. In the Simplex algorithm, the initial vector of simplex in parameter space is used with offsets of +5.0° and +5.0 pixels for the multiresolution approach. In the present method, these values are ±5.0° and +5.0 pixels for the pre-registration step and +1.5° and +1.0 pixels for the fine registration. Tolerance for the termination condition is set to be 0.1° and 0.1 pixels for both methods.

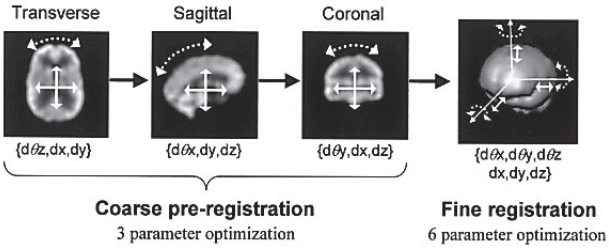

Fig. 1 Diagram of the 2D pre-registration strategy in the present method. The 2D image matching as a coarse pre-registration with a smaller number of parameters is performed in the transverse plane ($d\theta z$, dx, dy), sagittal plane ($d\theta x$, dy, dz) and coronal plane ($d\theta y$, dx, dz); all six parameters were then optimized as fine registration. Coarse pre-registration was performed with a half matrix size by voxel averaging to increase the computational efficiency.

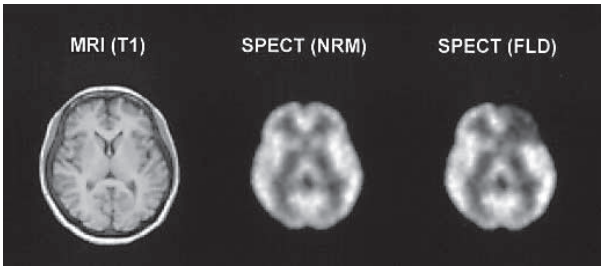

Fig. 2 Typical simulation data. MRI-T1 image and simulated SPECT images of a normal perfusion model (NRM) and a pathological perfusion model with frontal lobe defect (FLD). SPECT images were smoothed using a Gaussian filter with 8-mm FWHM to remove statistical noise.

Simulation data

Our simulation was based on realistic SPECT data from T1-weighted MRI images. The simulation used seven MRI data. Table 1 summarizes the MRI image parameters. They are described later in the section regarding the clinical study. Each MRI image was segmented into gray matter (GM), white matter (WM), and cerebrospinal fluid (CSF) using SPM99[27] software. The Renkin-Crone equation[28,29] provided the GM/WM ratio to be approximately 2.33 with corresponding cerebral blood flow (80 ml/100 g/min for GM and 20 ml/100 g/min for WM) and the permeability-surface area (PS) product of ECD (PS = 66 ml/100 g/min).[30] Consequently, the radioactivity ratio of GM, WM, and CSF was assumed to be 2.4 : 1.0 : 0.1 to simulate the brain perfusion pattern of ECD. In this simulation, we considered two perfusion models: a normal perfusion model (NRM) and a pathological perfusion model with frontal lobe defect (FLD). In the FLD model, the radioactivity of the defect region on GM was reduced to 60% of the normal value.

All perfusion images were resliced into 128 × 128 × 128 with a voxel size of 2.24 × 2.24 × 2.24 mm. They were then reprojected to generate the SPECT projection data with 2D Gaussian blurring (FWHM = 8 mm) and statistical noise. The effects of photon attenuation and scatter were not included in this simulation. The projection data were reconstructed by the ordered subsets-expectation maximization (OSEM) algorithm[31] (iteration = 3, subset size = 20). Figure 2 shows a typical simulation data set.

Evaluation of accuracy and precision using simulation data

The accuracy and precision of the algorithms was evaluated using simulation data. The simulation was performed using 100 independent trials with two types of initial mismatches which were randomly transformed within ±10° for rotations and ±17.92 mm (±8 voxel) for translations (refer to Type-I) and ±20° and ±40.32 mm (±18 voxel) (refer to Type-II). Registration was performed with the MRI-NRM SPECT and the MRI-FLD SPECT data sets. Accuracy and reproducibility of algorithms was evaluated by the mean and standard deviation (SD) of differences between true and estimated transformation parameters. Wong et al.[32] reported that a trained

Table 2 Mean errors of MI-based registration in MRI-NRM SPECT simulation

Algorithm	$d\theta x$ (deg)	$d\theta y$ (deg)	$d\theta z$ (deg)	dx (mm)	dy (mm)	dz (mm)	Success rate (%)	MI
Mismatch: Type-I[a)]								
Multiresolution approach	0.13 ± 0.15	0.03 ± 0.15	−0.04 ± 0.18	0.08 ± 0.12	−0.49 ± 0.12	0.57 ± 0.11	100	0.811
	(−0.37/0.86)	(−0.49/0.65)	(−0.80/0.72)	(−0.31/0.60)	(−0.95/0.09)	(0.13/1.03)		
Present method	0.12 ± 0.10	0.03 ± 0.10	−0.07 ± 0.11	0.09 ± 0.10	−0.49 ± 0.11	0.57 ± 0.10	100	0.811
	(−0.31/0.75)	(−0.29/0.68)	(−0.62/0.45)	(−0.29/0.47)	(−0.97/0.11)	(0.10/0.97)		
Mismatch: Type-II[b)]								
Multiresolution approach	0.15 ± 1.11	0.21 ± 1.80	0.06 ± 1.59	0.02 ± 0.88	−0.48 ± 0.41	0.51 ± 0.35	97.6	0.795
	(−16.6/14.6)	(−12.5/22.0)	(−8.03/23.4)	(−12.1/3.04)	(−5.92/4.87)	(−3.79/4.52)		
Present method	0.12 ± 0.17	0.06 ± 0.64	−0.07 ± 0.13	0.10 ± 0.20	−0.47 ± 0.18	0.52 ± 0.19	99.9	0.802
	(−0.74/2.46)	(−1.38/16.2)	(−0.84/0.54)	(−2.23/0.60)	(−1.13/0.32)	(−1.72/1.11)		

[a)] initial mismatch of ±10° for rotations and ±17.92 mm for translations
[b)] initial mismatch of ±20° for rotations and ±40.32 mm for translations
Values in parentheses represent the range of maximum possible error in each parameter

Table 3 Mean errors of NMI-based registration in MRI-NRM SPECT simulation

Algorithm	$d\theta x$ (deg)	$d\theta y$ (deg)	$d\theta z$ (deg)	dx (mm)	dy (mm)	dz (mm)	Success rate (%)	NMI
Mismatch: Type-I[a)]								
Multiresolution approach	0.15 ± 0.17	0.04 ± 0.15	−0.03 ± 0.18	0.10 ± 0.13	−0.40 ± 0.12	0.63 ± 0.11	100	1.079
	(−1.11/0.78)	(−0.79/0.72)	(−0.83/0.59)	(−0.35/0.69)	(−0.93/0.12)	(−0.10/1.02)		
Present method	0.12 ± 0.10	0.03 ± 0.10	−0.07 ± 0.10	0.09 ± 0.09	−0.49 ± 0.11	0.57 ± 0.10	100	1.080
	(−0.34/0.74)	(−0.24/0.55)	(−0.62/0.56)	(−0.26/0.50)	(−0.97/0.09)	(0.11/0.96)		
Mismatch: Type-II[b)]								
Multiresolution approach	0.20 ± 1.48	0.25 ± 2.04	0.14 ± 1.77	−0.00 ± 0.94	−0.18 ± 0.53	0.21 ± 0.36	97.4	1.078
	(−16.5/15.2)	(−8.93/22.5)	(−5.72/18.6)	(−4.56/0.99)	(−1.99/2.23)	(−1.12/1.50)		
Present method	0.13 ± 0.15	0.04 ± 0.17	−0.06 ± 0.15	0.04 ± 0.18	−0.19 ± 0.18	0.21 ± 0.17	100	1.080
	(−0.52/0.89)	(−1.82/0.78)	(−0.73/1.42)	(−0.27/0.25)	(−0.45/0.12)	(−0.09/0.43)		

[a)] initial mismatch of ±10° for rotations and ±17.92 mm for translations
[b)] initial mismatch of ±20° for rotations and ±40.32 mm for translations
Values in parentheses represent the range of maximum possible error in each parameter

Table 4 Mean errors of MI-based registration in MRI-FLD SPECT simulation

Algorithm	$d\theta x$ (deg)	$d\theta y$ (deg)	$d\theta z$ (deg)	dx (mm)	dy (mm)	dz (mm)	Success rate (%)	MI
Present method	0.17 ± 0.12	0.15 ± 0.11	−0.33 ± 0.12	0.29 ± 0.12	−0.72 ± 0.14	0.67 ± 0.11	100	0.796
	(−0.49/0.88)	(−0.22/0.71)	(−0.94/0.26)	(−0.16/0.81)	(−1.26/0.03)	(0.15/1.07)		

Values in parentheses represent the range of maximum possible error in each parameter

clinician can detect differences from the registration parameter of 4° in the x- and y-rotation angles, 2° in the z-rotation, 2 mm in the x- and y-translations, and 3 mm in the z-translation. Therefore, the registration was treated in this study as a success when all misregistration parameters were within the detection borderline. All data processing was performed on a PC (Pentium-4, 2.8 GHz, 512 MB memory).

Clinical application

The present methods based on MI and NMI were applied to the clinical data. The SPECT images were smoothed using a Gaussian filter (FWHM = 10 mm); the image count was truncated with a lower threshold of 5% of the maximum count.[19]

Seven human data of T1-weighted MRI and ECD-SPECT were used to evaluate the registration algorithm performance. One was an ictal/interictal SPECT study. Therefore, we analyzed eight MRI and SPECT data sets in all. The MRI images were acquired using gradient-echo sequence (echo time/repetition time, 4.4/11/4; flip angle, 15°) with a 1.0 T MRI scanner (Magnetom Impact Exper; Siemens Medical Solutions, Siemens AG). The SPECT measurement was performed using a triple-head gamma camera (MULTISPECT 3, Siemens Medical Solutions, Siemens AG) equipped with a high-resolution fan beam collimator. The acquisition matrix size was 128 × 128, with a pixel size of 2.46 × 2.46 mm. The number of

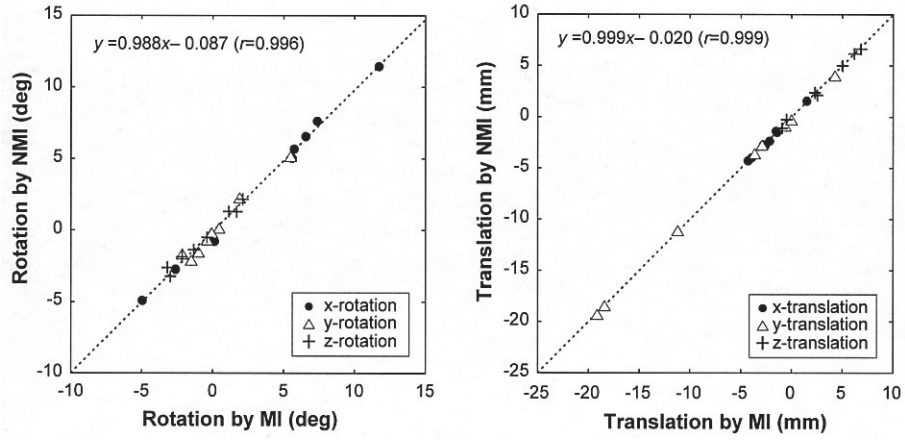

Fig. 3 Comparison of estimated rotational parameters (*left*) and translational parameters (*right*) with the MI- and NMI-based registration for all clinical data sets (n = 8).

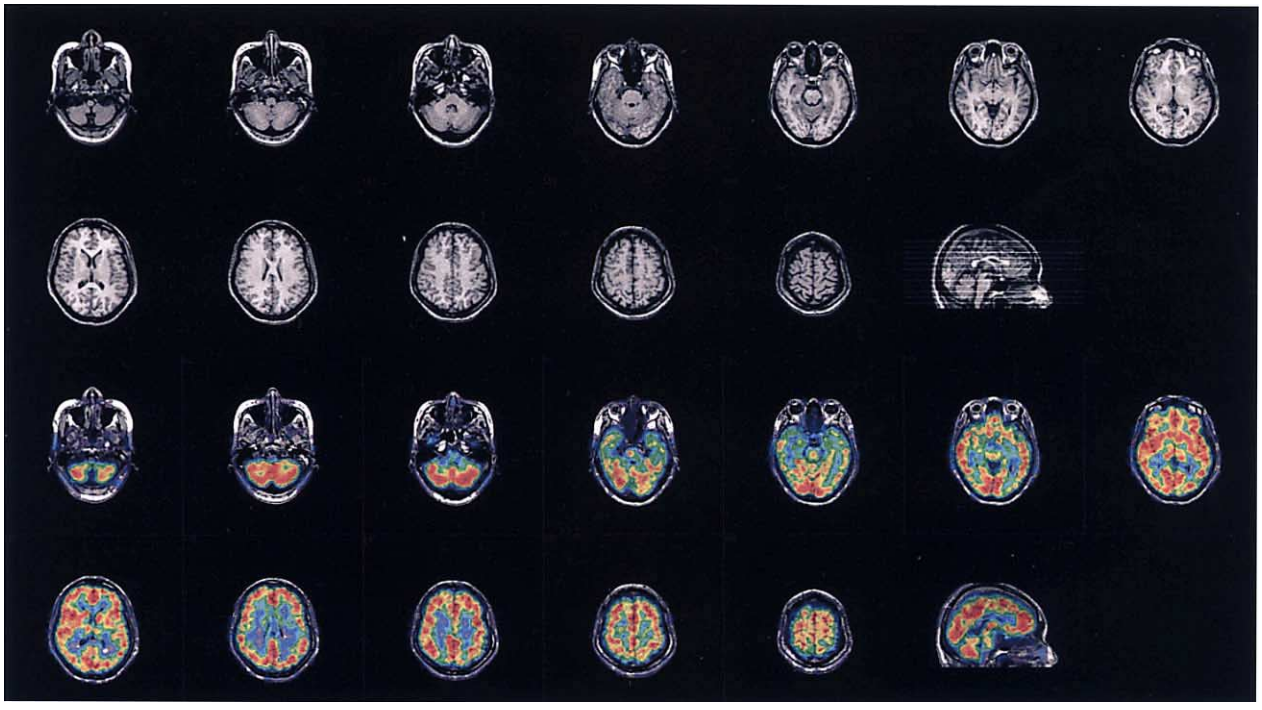

Fig. 4 Transverse images of MRI (*upper*) and fused images of the MRI and ECD-SPECT (*lower*) using the MI-based registration technique.

projection angles was 72; the acquisition time was 50 s/angle. Image reconstruction was performed using the filtered backprojection algorithm with the Hanning filter (0.7 cycles/cm). Chang's attenuation correction was performed using uniform μ-value (0.09 cm^{-1}). Table 1 summarizes the parameters of each image.

RESULTS

Validation of the simulated SPECT data

We examined the MI-based registration technique using MRI and NRM-SPECT images with no mismatch in advance to confirm the validity of the simulated SPECT data. The average of biases and SD (n = 7) in the multi-resolution approach were 0.07 ± 0.13°, 0.09 ± 0.07°, 0.00 ± 0.07° for *x*-, *y*- and *z*-rotations and 0.03 ± 0.05 mm, –0.30 ± 0.21 mm, 0.64 ± 0.14 mm for *x*-, *y*- and *z*-translations, respectively. Those in the present method were 0.17 ± 0.23°, –0.04 ± 0.19°, –0.07 ± 0.18° for *x*-, *y*- and *z*-rotations and 0.06 ± 0.07 mm, –0.36 ± 0.19 mm, 0.58 ± 0.14 mm for *x*-, *y*- and *z*-translations, respectively. Small offsets were observed in the *y*- and *z*-axis translation.

Accuracy and precision for MI-based registration technique

Table 2 shows mean errors of the MI-based registration technique in MRI-NRM SPECT simulation. The success rate of registration, mean MI value and the range of maximum possible error are also presented. In the case of Type-I (±10° and ±17.92 mm), no significant differences were found between the results of the multiresolution approach and the present method. No biases were observed in either method (≤0.13° and ≤0.57 mm for the multiresolution approach; ≤0.12° and ≤0.57 mm for the present method); the SDs were very small (≤0.18° and ≤0.12 mm for the multiresolution approach; ≤0.11° and ≤0.11 mm for the present method). The range of maximum possible error was within about ±1.0° and ±1.0 mm in both methods. All simulations (700 trials) were successful. The average run times for the multiresolution approach and the present method were 25 ± 6 and 31 ± 4 s, respectively.

In the case of Type-II (±20° and ±40.32 mm), the present method yielded better results in terms of accuracy and precision in comparison with the multiresolution approach. The SDs for the multiresolution approach (≤1.80° and ≤0.88 mm) were markedly larger than those for the present method (≤0.64° and ≤0.20 mm). The success rate for the present method was 99.9% (one of 700 trials failed) which was higher than 97.6% (17 of 700 trials failed) for the multiresolution approach. With the multiresolution approach, the maximum possible errors ranged from −16.6° to 23.4° for rotations and from −12.1 mm to 4.87 mm for translations. With the present method, they ranged from −1.38° to 16.2° for rotations and from −2.23 mm to 1.11 mm for translations. The 2D-coarse preregistration strategy provided a large capture range and was more robust with respect to the large initial mismatch.

Accuracy and precision for NMI-based registration technique

Table 3 shows mean errors of the NMI-based registration technique in the MRI-NRM SPECT simulation. Overall, the NMI showed the same tendency as the MI results. Comparison of the accuracy and precision for the multiresolution approach and the present method using Type-I showed no significant differences in any parameters. All simulations were successful in both methods.

However, in the case of Type-II, the present method exhibited better accuracy and precision than the multiresolution approach. The SDs for the multiresolution approach (≤2.04° and ≤0.94 mm) were markedly larger than those for the present method (≤0.17° and ≤0.18 mm). All simulations were successful with the present method, whereas the success rate was 97.4% (18 of 700 trials failed) with the multiresolution approach. The NMI accuracy and precision were almost equivalent to those of MI in our simulation condition. No differences were found between the average run times of NMI and MI.

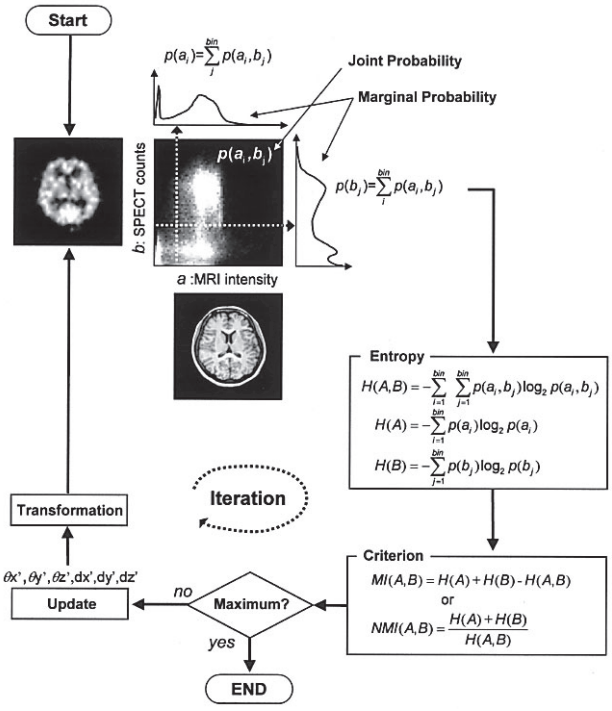

Fig. 5 The procedure of image registration based on MI or NMI.

The effect of defect region

Table 4 shows mean errors of the present method based on the MI criterion in the MRI-FLD SPECT simulation using Type-I. We found only minor differences between the registration results of the MRI-NRM SPECT simulation (Table 2) and the MRI-FLD SPECT simulation (Table 4). The biases were very small (≤0.33° and ≤0.72 mm), and the SDs for the present method were within 0.12° and 0.14 mm. The simulation revealed that frontal lobe defect has little influence on the registration accuracy and reproducibility.

Results of clinical application

Figure 3 shows a comparison of estimated registration parameters for rotation and translation using the MI- and NMI-based registration algorithms for all subjects. The rotational parameters ranged from −5° to 12°; the translational parameter ranged from −19 to 7 mm. No significant differences were shown between the two registration methods ($y_{NMI} = 0.988x_{MI} - 0.087$, r = 0.996 for rotations; $y_{NMI} = 0.999x_{MI} - 0.020$, r = 0.999 for translations). Figure 4 shows the MRI images and fused images of MRI-T1 and ECD-SPECT. The display shows good quality of the match for internal brain structures and brain surfaces. The method registered the SPECT and the MRI for all subjects with an accuracy that we could not fault by visual inspection.

DISCUSSION

The concept of mutual information (MI) is a measure originating from information theory or telecommunication systems; the concept of MI can also be used as a similarity measure for two images. Normalized mutual information (NMI) is also proposed as a robust similarity measure for variation of an overlapped region of two images. The MI- and NMI-based registration has become the most investigated technique for medical image registration during recent years.[14–23]

In general, an optimization algorithm cannot guarantee reaching a global optimum. The value can easily be trapped in local optima. For that reason, the choice of optimization strategy strongly influences the registration results. Maes et al.[33] investigated the performance of six optimization algorithms: Simplex, Powell, steepest gradient-descent, conjugate-gradient, quasi-Newton, Levenberg-Marquardt. They reported that the Powell algorithm yielded the best results and the Simplex algorithm provided the second best results. Bernon et al.[34] also performed a comparative study of the Powell and Simplex algorithms for multimodal surface matching. They reported that the Simplex algorithm provided the best results. The Powell method optimizes each parameter using an iterative 1D linear search, whereas the Simplex algorithm generally optimizes all six parameters simultaneously. This study implemented an alternative approach of a 3D registration technique including 2D image matching as coarse pre-registration using the Simplex algorithm. The 2D coarse pre-registration optimizes the only three parameters in the transverse, sagittal and coronal planes, respectively. Subsequently, all six parameters were then optimized as fine registration, as shown in Figure 1. Maes et al.[14] and Lin et al.[35] suggested that in-plane parameters ($d\theta z$, dx, dy) could be determined more quickly as independent of the initial conditions in brain study. For that reason, we performed transverse plane ($d\theta z$, dx, dy) matching first; sagittal plane ($d\theta x$, dy, dz) matching and coronal plane ($d\theta y$, dx, dz) matching were performed sequentially in the present method. The value of $d\theta y$ corresponds to the difference between the loading angle of a patient into the MRI and SPECT scanner. It is expected to be smaller than the value of $d\theta x$, as shown in Figure 3. Therefore, performing coronal plane matching after sagittal plane matching seemed reasonable. When comparing the multiresolution approach and the present method regarding its accuracy and precision with the initial mismatch of ±10° and ±17.92 mm (Type-I), no siginificant differences were shown between the two methods (Table 2 and Table 3). Our simulation study showed that biases in y-axis translation (dy) and z-axis translation (dz) were slightly larger than that of x-axis translation (dx) in both methods. These anisotropic biases were probably introduced by the initial offset of the simulation data. Considering the initial offset, the biases would be isotropic in each direction. On the other hand, the present method improved the accuracy and precision in comparison with the multiresolution approach when the initial mismatch was ±20° and ±40.32 mm (Type-II). The success rate in the present method was 99.9%, which was higher than 97.6% in the multiresolution approach. An identical tendency was observed in results by the NMI-based registration (100% for the present method, 97.4% for the multiresolution approach). Simulation revealed that the 2D-coarse pre-registration strategy in the present method provided a large capture range. We believe that the 2D pre-registration strategy can improve the registration robustness to a large initial mismatch. We focused on brain image registration using the rigid-body transformation model in this study, but cardiac and abdominal thorax image registration is a more complex problem because of the non-rigid and mixed motions of the heart and the thorax structures. The nonlinear registration based on MI or NMI has been reported to register thorax MRI images.[21,41] However, it is unclear whether the present 2D pre-registration technique is effective or not in cardiac and abdominal thorax image registration.

We compared the accuracy and precision of the NMI-based registration with that of the MI-based registration. As mentioned above, the NMI criterion is an insensitive measure for overlapping regions of two images. For that reason, the capture range of the NMI was expected to be larger than that of the MI. However, we found almost equivalent performance for MI and NMI registration results. Grove et al.[36] investigated the performance of several registration algorithms (MI, NMI, Correlation ratio, Woods criterion) for MRI/SPECT registration using realistic simulated SPECT data. They also observed no significantly differences between the MI and NMI results. Additional studies are required to prove the robustness of the NMI criterion with a larger initial mismatch.

The accuracy and speed of registration generally present a tradeoff relationship. However, the present method showed only about a 1.2-fold increase in the average run time in comparison with the multiresolution approach. Pre-registration optimized the only three parameters with small matrix size; these contributed to increasing the computational efficiency. Pluim et al.[37] reported that interpolation-induced local minima were found on a registration function for translation in the slice direction. Reslicing of the floating volume is affected by the interpolation effect. Consequently, the choice of method appears to have some influence on cost function smoothness. Various interpolation schemes were proposed including B-Spline interpolation,[38] convolution-based interpolation[39] and partial volume interpolation.[14] Meijering et al.[39] reported that spline interpolation is preferable to convolution-based interpolation, but we employed the simple trilinear interpolation scheme because of its accuracy and relatively low computational cost. Tsao[40]

investigated the effect of various interpolation schemes in MRI/ECD-SPECT registration. He reported that interpolation artifacts were unlikely to be a major source of registration error unless used with an extreme number of bins (e.g. > 128). Our simulation results also suggested a negligible interpolation effect even with use of simple trilinear interpolation.

CONCLUSION

We implemented improved 3D co-registration techniques based on mutual information (MI) and normalized mutual information (NMI), including a 2D image matching as the coarse pre-registration. Accuracy and precision of the present method were evaluated using simulated data and clinical data. The present method with the 2D coarse pre-registration strategy improved registration robustness. The accuracy and precision of NMI were almost equivalent to the MI in our simulation condition. The choice of optimization strategy was more important than the choice of the registration criterion (MI or NMI). Performance of the present method offers sufficient accuracy and reproducibility for MRI-SPECT registration.

ACKNOWLEDGMENT

Part of this study was presented at the European Association of Nuclear Medicine Congress (August 23–27, 2003, Amsterdam).

APPENDIX

The procedure of image registration based on MI and NMI is illustrated in Figure 5. First, 2D histogram $h(a_i,b_j)$ is calculated from the two variables (e.g. a_i = MRI, b_j = SPECT). The joint probability distribution $p(a_i,b_j)$ can be calculated simply by normalizing the 2D histogram as the following equation:

$$p(a_i,b_j) = \frac{h(a_i,b_j)}{\sum_{i=1}^{bin}\sum_{j=1}^{bin} h(a_i,b_j)}, \quad \text{(A1)}$$

where *bin* represents the size of the 2D histogram. The denominator of Eq. (A1) is a constant value, so that the distribution pattern of $p(a_i,b_j)$ is identical to that of $h(a_i,b_j)$. The marginal probability $p(a_i)$ and $p(b_j)$ can be calculated by summing $p(a_i,b_j)$ over b and a, respectively, as the following equations:

$$p(a_i) = \sum_{j=1}^{bin} p(a_i,b_j), \quad \text{(A2)}$$

$$p(b_j) = \sum_{i=1}^{bin} p(a_i,b_j). \quad \text{(A3)}$$

Subsequently, the joint entropy and marginal entropy are given by the following equations:

$$H(A,B) = -\sum_{i=1}^{bin}\sum_{j=1}^{bin} p(a_i,b_j)\log_2 p(a_i,b_j), \quad \text{(A4)}$$

$$H(A) = -\sum_{i=1}^{bin} p(a_i)\log_2 p(a_i), \quad \text{(A5)}$$

$$H(B) = -\sum_{j=1}^{bin} p(b_j)\log_2 p(b_j). \quad \text{(A6)}$$

Mutual information (MI) and normalized mutual information (NMI) can be calculated as follows:

$$MI(A,B) = H(A) + H(B) - H(A,B). \quad \text{(A7)}$$

$$NMI(A,B) = \frac{H(A) + H(B)}{H(A,B)}. \quad \text{(A8)}$$

When the algorithm does not reach the maximum MI (or NMI) value, the registration parameters are updated by the optimization algorithm (e.g. Simplex algorithm). In our method, three parameters are optimized in the 2D pre-registration; all six parameters are optimized in the fine registration. The floating image (SPECT image) is transformed using the updated parameters, and the above procedure is then repeated until convergence.

REFERENCES

1. Wahl RL, Quint LE, Cieslak RD, Aisen AM, Koeppe RA, Meyer CR. "Anatometabolic" tumor imaging: fusion of FDG PET with CT or MRI to localize foci of increased activity. *J Nucl Med* 1993; 34: 1190–1197.
2. Pohjonen HK, Savolainen SE, Nikkinen PH, Poutanen VP, Korppi-Tommola ET, Liewendahl BK. Abdominal SPECT/MRI fusion applied to the study of splenic and hepatic uptake of radiolabeled thrombocytes and colloids. *Ann Nucl Med* 1996; 10: 409–417.
3. Forster GJ, Laumann C, Nickel O, Kann P, Rieker O, Bartenstein P. SPET/CT image co-registration in the abdomen with a simple and cost-effective tool. *Eur J Nucl Med Mol Imaging* 2003; 30: 32–39.
4. Suga K. Technical and analytical advances in pulmonary ventilation SPECT with xenon-133 gas and Tc-99m-Technegas. *Ann Nucl Med* 2002; 16: 303–310.
5. Takahashi Y, Murase K, Higashino H, Mochizuki T, Motomura N. Attenuation correction of myocardial SPECT images with X-ray CT: effects of registration errors between X-ray CT and SPECT. *Ann Nucl Med* 2002; 16: 431–435.
6. Zaidi H, Montandon ML, Slosman DO. Magnetic resonance imaging-guided attenuation and scatter corrections in three-dimensional brain positron emission tomography. *Med Phys* 2003; 30: 937–948.
7. Woods RP, Mazziotta JC, Cherry SR. MRI-PET registration with automated algorithm. *J Comput Assist Tomogr* 1993; 17: 536–546.
8. Ardekani BA, Braun M, Hutton BF, Kanno I, Iida H. A fully automatic multimodality image registration algorithm. *J Comput Assist Tomogr* 1995; 19: 615–623.
9. Barnden L, Kwiatek R, Lau Y, Hutton B, Thurfjell L, Pile K, et al. Validation of fully automatic brain SPET to MR co-

registration. *Eur J Nucl Med* 2000; 27: 147–154.
10. West J, Fitzpatrick JM, Wang MY, Dawant BM, Maurer CR Jr, Kessler RM, et al. Comparison and evaluation of retrospective intermodality brain image registration techniques. *J Comput Assist Tomogr* 1997; 21: 554–566.
11. Strother SC, Anderson JR, Xu XL, Liow JS, Bonar DC, Rottenberg DA. Quantitative comparisons of image registration techniques based on high-resolution MRI of the brain. *J Comput Assist Tomogr* 1994; 18: 954–962.
12. Collignon A, Maes F, Delaere D, Vandermeulen D, Suetens P, Marchal G. Automated multi-modality image registration based on information theory. In Bizais Y, Barillot C, Di Paola R (eds), *Information Processing in Medical Imaging*. Dordrecht, Kluwer Academic Publishers, 1995: 263–274.
13. Viola P, Wells WM III. Alignment by maximization of mutual information. In *Proc. 5th Int. Conf. Computer Vision,* Cambridge, MA, 1995: 16–23.
14. Maes F, Collignon A, Vandermeulen D, Marchal G, Suetens P. Multimodality image registration by maximization of mutual information. *IEEE Trans Med Imaging* 1997; 16: 187–198.
15. Wells WM III, Viola P, Atsumi H, Nakajima S, Kikinis R. Multi-modal volume registration by maximization of mutual information. *Med Image Anal* 1996; 1: 35–51.
16. Studholme C, Hill DL, Hawkes DJ. Automated three-dimensional registration of magnetic resonance and positron emission tomography brain images by multiresolution optimization of voxel similarity measures. *Med Phys* 1997; 24: 25–35.
17. Skalski J, Wahl RL, Meyer CR. Comparison of mutual information-based warping accuracy for fusing body CT and PET by 2 methods: CT mapped onto PET emission scan versus CT mapped onto PET transmission scan. *J Nucl Med* 2002; 43: 1184–1187.
18. Thurfjell L, Lau YH, Andersson JL, Hutton BF. Improved efficiency for MRI-SPET registration based on mutual information. *Eur J Nucl Med* 2000; 27: 847–856.
19. Zhu YM, Cochoff SM. Influence of implementation parameters on registration of MR and SPECT brain images by maximization of mutual information. *J Nucl Med* 2002; 43: 160–166.
20. Studholme C, Hill DLG, Hawkes DJ. An overlap invariant entropy measure of 3D medical image alignment. *Pattern Recognition* 1999; 32: 71–86.
21. Denton ER, Sonoda LI, Rueckert D, Rankin SC, Hayes C, Leach MO, et al. Comparison and evaluation of rigid, affine, and nonrigid registration of breast MR images. *J Comput Assist Tomogr* 1999; 23: 800–805.
22. Holden M, Hill DL, Denton ER, Jarosz JM, Cox TC, Rohlfing T, et al. Voxel similarity measures for 3-D serial MR brain image registration. *IEEE Trans Med Imaging* 2000; 19: 94–102.
23. Radau PE, Slomka PJ, Julin P, Svensson L, Wahlund L-O. Evaluation of linear registration algorithms for brain SPECT and the errors due to hypoperfusion lesions. *Med Phys* 2001; 28: 1660–1668.
24. Shannon CE. A mathematical theory of communication. *Bell System Technical Journal* 1948; 27: 379–423/623–656.
25. Nelder JA, Mead R. A simplex method for function minimization. *Comput J* 1965; 308–313.
26. Press WH, Teukolsky SA, Vetterling WT, Flannery BP. *Numerical Recipes in C: Japanese Edition*. Gijutsu Hyoron Sha, 1993: 295–299.
27. Friston KJ, Holmes AP, Worsley KJ, Poline JP, Frith CD, Frackowiak RSJ. Statistical parametric maps in functional imaging: a general linear approach. *Human Brain Mapping* 1995; 2: 189–210.
28. Renkin EM. Transport of potassium-42 from blood to tissue in isolated mammalian skeletal muscles. *Am J Physiol* 1959; 197: 1205–1210.
29. Crone C. The permeability of capillaries in various organs as determined by use of the 'indicator diffusion' method. *Acta Physiol Scand* 1963; 58: 292–305.
30. Tsuchida T, Yonekura Y, Nishizawa S, Sadato N, Tamaki N, Fujita T, et al. Nonlinearity correction of brain perfusion SPECT based on permeability-surface area product model. *J Nucl Med* 1996; 37: 1237–1241.
31. Hudson HM, Larkin RS. Accelerated image reconstruction using ordered subsets of projection data. *IEEE Trans Med Imaging* 1994; MI-13: 601–609.
32. Wong JC, Studholme C, Hawkes DJ, Maisey MN. Evaluation of the limits of visual detection of image misregistration in a brain fluorine-18 fluorodeoxyglucose PET-MRI study. *Eur J Nucl Med* 1997; 24: 642–650.
33. Maes F, Vandermeulen D, Suetens P. Comparative evaluation of multiresolution optimization strategies for multimodality image registration by maximization of mutual information. *Med Image Anal* 1999; 3: 373–386.
34. Bernon JL, Boudousq V, Rohmer JF, Fourcade M, Zanca M, Rossi M, et al. A comparative study of Powell's and Downhill Simplex algorithms for a fast multimodal surface matching in brain imaging. *Comput Med Imaging Graph* 2001; 25: 287–297.
35. Lin KP, Huang SC, Yu DC, Melega W, Barrio JR, Phelps ME. Automated image registration for FDOPA PET studies. *Phys Med Biol* 1996; 41: 2775–2788.
36. Grova C, Biraben A, Scarabin J-M, et al. A methodology to validate MRI/SPECT registration methods using realistic simulated SPECT data. Niessen W, Viergever M (eds), In MICCAI 2001, *Lecture notes in Computer Science* 2001; 2208: 275–282.
37. Pluim JP, Maintz JB, Viergever MA. Image registration by maximization of combined mutual information and gradient information. *IEEE Trans Med Imaging* 2000; 19: 809–814.
38. Thevenaz P, Unser M. A pyramid approach to sub-pixel image fusion based on mutual information. *Proc IEEE Int Conf on Imag Proc ICIP '96* 1996; 1: 261–264.
39. Meijering EH, Niessen WJ, Viergever MA. Quantitative evaluation of convolution-based methods for medical image interpolation. *Med Image Anal* 2001; 5: 111–126.
40. Tsao J. Interpolation artifacts in multimodality image registration based on maximization of mutual information. *IEEE Trans Med Imaging* 2003; 22: 854–864.
41. Carrillo A, Duerk JL, Lewin JS, Wilson DL. Semiautomatic 3-D image registration as applied to interventional MRI liver cancer treatment. *IEEE Trans Med Imaging* 2000; 19: 175–185.